Chemical Engineering Journal 165 (2010) 916–923

Contents lists available at ScienceDirect

Chemical Engineering Journal

journal homepage: www.elsevier.com/locate/cej

Highly selective 1-heptene isomerization over vanadium grafted mesoporous molecular sieve catalysts

Shuangquan Hu [a], Dapeng Liu [a], Lusi Li [a], Zhen Guo [a], Yuanting Chen [a], Armando Borgna [b], Yanhui Yang [a,*]

[a] School of Chemical and Biomedical Engineering, Nanyang Technological University, 62 Nanyang Drive, N1.2-B1-18, Singapore 637459, Singapore
[b] Institute of Chemical and Engineering Sciences (ICES), A*STAR, 1 Pesek Road, Jurong Island, Singapore 627833, Singapore

ARTICLE INFO

Article history:
Received 6 March 2010
Received in revised form
24 September 2010
Accepted 2 October 2010

Keywords:
Alkene isomerization
Vanadium
Grafting
Pore diameter
Pore structure

ABSTRACT

Mesoporous molecular sieve supported vanadium catalysts (V-MCM-41, V-SBA-15 and V-TUD-1) with different pore structures and pore sizes were prepared via a post-synthesis grafting method using atomic layer deposition. Nitrogen physisorption and X-ray diffraction demonstrated that ordered mesoporous structures for all samples were attained after grafting procedures. UV–vis and UV–Raman spectroscopies suggested that highly dispersed vanadium units were formed on the pore wall surface. Ammonia temperature-programmed desorption and IR spectroscopy of adsorbed pyridine suggested the existence of mild acidity, containing both Lewis and Brønsted sites; the ratios of Lewis/Brønsted acid depended on the structure of the catalyst support. The isomerization of 1-heptene was employed as a reaction probe to characterize the acid properties of these catalysts with moderate acid strengths. No methyl migration isomerization was observed since a stronger acidity was required. Conversion as high as 92% at 600 K and isomer selectivity over 90% (mainly double bond shift products) over the V-SBA-15 catalyst were achieved. The catalytic performances, including activities, selectivities, 2-heptene to 3-heptene ratios, and *cis*-heptene/*trans*-heptene ratios, over different mesoporous supported catalysts were compared and discussed in detail. The catalyst deactivation was also explored.

1. Introduction

Isomerization of alkanes and alkenes is of essential importance for producing high quality transportation fuels since it leads to an increase of the octane number, improving the fuel resistance to knock [1–10]. Alkenes possess higher octane number as compared to the corresponding alkanes. In addition, alkenes with internal C=C double bonds have higher octane number than those with terminal C=C double bonds [2]. It is important to stress that alkenes are the major components of the gasoline pool produced by fluid catalytic cracking (FCC) of naphtha [11,12]. Currently, 80% of gasoline supply is from FCC process, containing about 50% of alkenes [13,14]. Therefore, the isomerization of alkenes is of both scientific and technological interest.

On the other hand, hydrodesulfurization (HDS) is a necessary step to lower the sulfur content in gasoline required by strict environmental regulations [12,15]. However, HDS process tends to saturate the alkenes in FCC naphtha, resulting in a lower octane number of fuel [12,13]. Interestingly, Toba et al. reported that olefinic compounds are able to resist being hydrogenated under HDS conditions if the C=C double bond shifts from terminal- to internal-position [16]. Along this line, the study of alkene isomerization to shift the terminal double bond to an internal one will be essential for maintaining the quality of gasoline products from FCC naphtha cracking.

A vast number of studies on alkene isomerization have been carried out using both zeolites and mesoporous materials as catalysts or catalyst supports [12,13,17,18]. Investigating the effect of pore size and structure on the isomerization activity and selectivity is attracting growing attention [19–22]. For instance, the effect of zeolite pore sizes and structures on the selectivity towards double bond shift isomerization and *cis*/*trans* isomer ratios have been reported [12,17,23]. Shi and Shen reported that using highly ordered MCM-41 as supports results in higher amount of skeletal isomers as compared to the traditional γ-Al_2O_3 supports in the 1-hexene isomerization [13].

Most of alkene isomerization studies have been devoted to the isomerization of butene and hexene [1,2,12,13,15,17,18,23,24]. Although heptene isomerization was rarely reported in literature, heptene represents one of the largest contributions to the alkene pool in FCC naphtha [25,26]. In a previous study, vanadium incorporated MCM-41 catalysts were successfully prepared and applied to the 1-heptene isomerization due to the moderate acid strength of vanadium sites [25]. However, the direct synthesis method causes

* Corresponding author. Tel.: +65 6316 8940; fax: +65 6794 7553.
E-mail address: yhyang@ntu.edu.sg (Y. Yang).

1385-8947/$ – see front matter © 2010 Elsevier B.V. All rights reserved.
doi:10.1016/j.cej.2010.10.001

a significant loss of vanadium active sites by burying them into the silicate framework of pore wall. Recently, a controlled post synthesis grafting method using atomic layer deposition (ALD) has been developed to prepare isolated vanadium sites highly dispersed on mesoporous material supports [27]. The key advantage is that all vanadium sites are exposed on the pore wall surface and accessible to the reactants. Another advantage of ALD method is that a strong interaction between vanadium sites and the support exists due to the formation of Si–O–V bonds. In the present work, isomerization of 1-heptene is carried out over vanadium grafted MCM-41, SBA-15 and TUD-1 catalysts prepared via this ALD technique. The effects of pore size and structure on the catalytic activity and selectivity are discussed in detail.

2. Experimental

2.1. Catalyst preparations

In a typical synthesis of siliceous MCM-41, 0.97 g of hexadecyltrimethyl-ammonium bromide (CTAB, >99%, Sigma) was dissolved in a mixture of 20 ml of ammonia solution ($NH_3{\cdot}H_2O$, 25%, VWR international) and 15 ml of deionized water. The surfactant solution was stirred till a clear solution was obtained. 4.5 g of tetraethyl orthosilicate (TEOS, 98%, Acros Organics) was added dropwise under vigorous stirring. After additional stirring for 120 min, the synthesis gel was transferred into a Teflon-lined stainless steel autoclave and placed in an oven at 393 K for 48 h. After cooling to room temperature, the resulting powder was recovered by filtration, washed with deionized water and dried under ambient conditions.

The siliceous SBA-15 was synthesized following a well-established procedure under acidic conditions using TEOS and a tri-block copolymer as silica precursor and template, respectively [28]. 2 g of the tri-block copolymer poly(ethylene glycol)-block-poly(propylene glycol)-block-poly(ethylene glycol) (P123, EO_{20}-PO_{70}-EO_{20}, Aldrich) was dissolved in 12.5 ml of deionized water under vigorous stirring. Upon the dissolving of P123, 35 ml of 0.29 M HCl solution (37%, Sigma–Aldrich) was added. The mixture was then stirred for 1 h at room temperature followed by adding 4.5 g of TEOS dropwise under stirring. After stirring at 313 K for 24 h, the white suspension was transferred into a polypropylene bottle and placed in an oven at 373 K for 24 h. The resulting powder was recovered by filtration, washed with deionized water and dried under ambient conditions.

The siliceous TUD-1 was synthesized following the method reported by Hamdy et al. [29]. In a typical preparation, 1.0 g of deionized water was added to 10 g of TEOS followed by adding 7.2 g of triethanolamine (TEA, >98.5%, Fluka) and 1.8 g of deionized water dropwise under vigorous stirring. After stirring for 30 min, 10.1 g of tetraethyl ammonium hydroxide (TEAOH, 35%, Aldrich) was added. The mixture was aged at room temperature for 24 h, dried at 373 K for 24 h, and hydrothermally treated in a Teflon-lined stainless steel autoclave at 453 K for 8 h. The pre-dried MCM-41, SBA-15, and TUD-1 were heated at a constant rate from room temperature to 873 K over 20 h under He and held for 1 h under the same condition, followed by calcination at 873 K for 5 h in air to remove the residual organic template.

The vanadium grafted mesoporous catalysts were synthesized following a slightly modified controlled post grafting method through ALD [27]. Vanadium (V) oxytriethoxide precursor was dissolved in anhydrous toluene (HPLC grade, Fisher Scientific). The as-calcined siliceous mesoporous material was suspended in anhydrous toluene and refluxed under an inert N_2 atmosphere for 5 h to completely remove the adsorbed moisture. A certain amount of the vanadium precursor in anhydrous toluene solution was added dropwise into the suspension and kept stirring under reflux and N_2 atmosphere for 12 h. The resulting mixture was cooled, filtered, and washed with anhydrous toluene to remove any un-reacted vanadium precursor and by-products. The powder was dried at room temperature overnight and calcined at 813 K for 6 h to obtain the final vanadium grafted catalysts. The catalyst was denoted as *x*V-support (I.E. 3V-MCM-41) where *x* represents the weight percentage of vanadium in a V-MCM-41 catalyst.

2.2. Catalyst characterizations

Nitrogen adsorption–desorption isotherms were measured at 77 K on a Quantachrome Autosorb-6b static volumetric instrument. Prior to the measurement, samples were outgassed at 623 K under vacuum. The specific surface area was calculated by BET method. The pore size and pore size distribution were calculated by BJH method using the desorption branch. X-ray diffraction (XRD) measurements were conducted on a Bruker Axs D8 X-ray diffractometer (Cu Kα, λ = 0.154 nm, 40 kV, 30 mA) under ambient conditions. Coke formation was quantitatively analyzed on a Perkin–Elmer Pyris Diamond TG/DTA instrument under air atmosphere at a heating rate of 10 K/min in the temperature range of 298–1073 K.

Diffuse reflectance UV–vis spectra were recorded on a VARIAN 5000 UV–vis–NIR spectrophotometer in the range of 200–800 nm. All samples were dried at 373 K overnight before carrying out the test. UV–Raman spectra were recorded using an excitation wavelength of 325 nm on a RENISHAW INVIA Raman Microscope under ambient conditions. Samples were pre-dried at 423 K overnight to remove the surface moisture. A laser output of 30 mW was used and the maximum incident power at the sample was approximately 6 mW to minimize the laser-induced alterations of the sample.

The acidity was investigated using temperature-programmed desorption of ammonia (TPD) on a Quantachrome Autosorb-1C instrument. The samples were pretreated at 773 K under helium followed by NH_3 adsorption at 373 K. After removing physisorbed NH_3 under helium flow, TPD analysis was carried out in the temperature range of 373–950 K at a ramping rate of 5 K/min under flowing helium. The desorbed gas was analyzed using a thermal conductivity detector (TCD).

In situ adsorbed pyridine infrared (IR) spectra were recorded with a Bruker EMX spectrometer in transmission mode. Samples were mixed with KBr, pressed into thin wafers and placed inside the cell. Prior to the measurement, the sample was dehydrated at 523 K for 1 h followed by introducing pyridine (PY) vapors at 323 K till saturation. Helium was used to purge the sample for 30 min at various temperatures, 323, 373, 423, and 473 K. Spectra were obtained at room temperature after background removal.

2.3. Catalytic reactions

1-Heptene isomerization was employed as a model reaction to study the catalytic properties of the as-prepared vanadium catalysts. Typically, 200 mg of catalyst was loaded in a down-flow quartz micro-reactor equipped with a thermocouple. The reactor was installed vertically inside a 35 mm i.d. tubular furnace controlled by a PID temperature controller. All gases were fed by calibrated mass flow controllers. Before each reaction experiment, the catalyst was pre-treated in situ under 20 ml/min of helium stream at 673 K for 1 h. 1-Heptene with a constant flow rate of 0.01 ml/min was fed by a HPLC pump. The partial pressure of 1-Heptene was kept constant (4.2%) using He as balance. The weight hourly space velocity (WHSV) was maintained at 2 h^{-1}. The whole system, including pipelines, was heated at 393 K to vaporize the 1-heptene and avoid condensation of the products. The feed and products were analyzed by an on-line gas chromatograph (Agilent 6890) equipped with FID detector and PONA column.

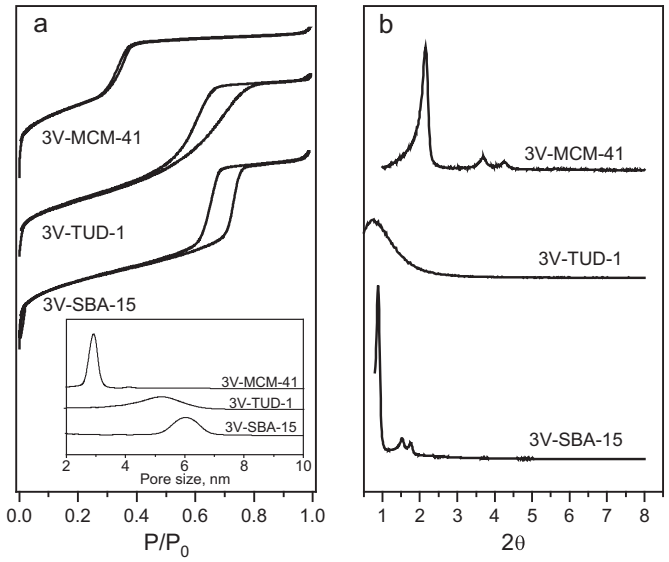

Fig. 1. (a) Nitrogen physisorption and (b) XRD patterns of vanadium grafted catalysts.

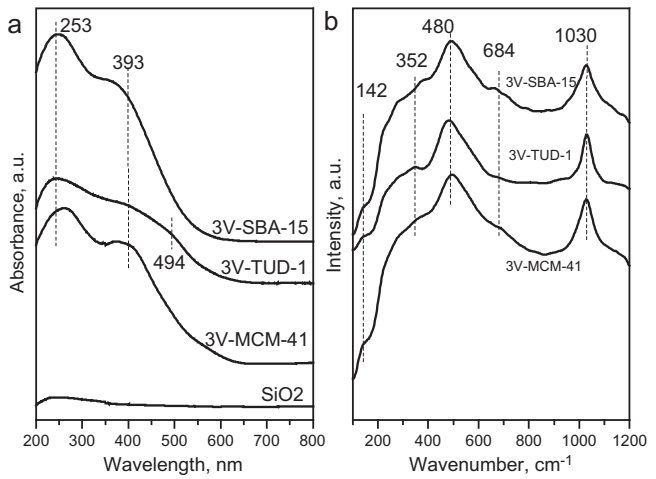

Fig. 2. (a) Diffuse reflectance UV–vis spectra and (b) UV–Raman spectra of vanadium grafted catalysts.

3. Results and discussion

3.1. Catalysts characterization

The nitrogen physisorption isotherms and the corresponding pore size distributions are shown in Fig. 1(a). All vanadium grafted samples (3V-MCM-41, 3V-TUD-1 and 3V-SBA-15) exhibit type IV isotherms according to the IUPAC classification, corresponding to mesoporous materials. For 3V-MCM-41, the capillary condensation shows a sharp step increase in nitrogen uptake in the relative pressure (P/P_0) range of 0.3–0.4 without adsorption–desorption hysteresis loop, suggesting highly ordered mesoporous structure with uniform channel size. 3V-TUD-1 shows a well-defined step in the P/P_0 range of 0.45–0.8 with a H1-type hysteresis loop [29]. The isotherm of 3V-SBA-15 displays a step increase of nitrogen uptake in the P/P_0 range of 0.6–0.8 with a characteristic H1-type broad hysteresis loop, corresponding to a large-pore mesoporous material with 1D cylindrical channels [27,30]. The hysteresis loop suggests long mesopores limit the emptying and filling of accessible volume [31]. Due to the disordered sponge-like mesostructure, 3V-TUD-1 possesses a relatively wider pore size distribution as compared to that of 3V-MCM-41 and 3V-SBA-15 [32,33]. All vanadium-grafted samples show large pore volume, greater than 1.10 cm^3/g, as summarized in Table 1. V-MCM-41, V-TUD-1 and V-SBA-15 show significant different pore diameters, 2.9, 5.4 and 6.0 nm, respectively. The surface area decreases from 922 to 706.6 m^2/g in the following sequence: V-MCM-41, V-SBA-15 and V-TUD-1. The low-angle XRD patterns of various vanadium-grafted samples are shown in Fig. 1(b). The results suggest that long-range order of the mesostructure is well retained after grafting and calcination procedures. For V-MCM-41 and V-SBA-15, three distinct Bragg diffraction peaks indexed as (1 0 0), (1 1 0) and (2 0 0) planes can be discerned [30,34]. Only one relatively boarder diffraction peak can be observed for V-TUD-1, demonstrating the irregular mesostructure of TUD-1 [29].

The UV–vis spectra of V-MCM-41, V-SBA-15, and V-TUD-1 are shown in Fig. 2(a). The lack of absorbance in the range of 600–800 nm for all vanadium grafted samples is due to the absence of the characteristic d–d transitions of $(VO)^{2+}$ [21], suggesting the complete oxidation of vanadium precursors to V^{5+} oxidation state. All samples show two distinct bands at 253 and 393 nm, which are attributed to isolated vanadium species in a tetrahedral symmetry [35,36]. For V-MCM-41 and V-SBA-15, the absence of the 320 and 450 nm bands indicates that no polymeric V–O–V bond and V_2O_5 crystallites species exist in these samples [36]. A weak band at 494 nm is observed for 3V-TUD-1 which is contributed by the formation of V_2O_5 crystallites as a consequence of the polymerization of V species on TUD-1 surfaces [36]. The formation of polymeric V–O–V bonds may be due to the relatively lower density of OH groups on TUD-1 surfaces for grafting as the synthesis of TUD-1 usually employs a small amount of H_2O.

The Raman spectra of these samples are shown in Fig. 2(b). The samples are considered as partially hydrated as the measurements were carried out under ambient conditions. A strong band at ~1030 cm^{-1} can be assigned to the symmetric V=O stretching vibration of isolated VO_4 species [27,37–40], suggesting that most of vanadium species in the grafted samples are isolated VO_4. The bands at ~352 and ~480 cm^{-1} are contributed by the ν_s and ν_{as} bending modes of the surface VO_4 unit, respectively [40]. These results indicate that the vanadium sites on the support surfaces are mostly isolated VO_4 units. The weak bands at 142 and 684 cm^{-1} are assigned to the hydrated amorphous polymeric vanadium oxide species on the surfaces [27]. Due to the partially hydrated conditions, the band for V_2O_5 at 995 cm^{-1} may not be detected for 3V-TUD-1 which contains a small amount of V_2O_5 crystallites as suggested by UV–vis characterizations.

TPD of basic molecule such as ammonia is one of the most commonly used methods for determining surface acidity [41]. The position and area of the TPD peaks give information about the relative acid strength and number of acid sites, respectively. The TPD profiles of these vanadium grafted catalysts with same vanadium loading (3 wt.%) are shown in Fig. 3. Only one desorption peak at medium temperature range is found for all samples. The peak

Table 1
Physicochemical properties of the three type mesoporous catalysts and their Lewis/Brøsted acidity ratio.

Sample	BET surface area (m^2/g)	Pore volume (cm^3/g)	Pore diameter (nm)	Lewis/Brøsted acidity ratio
3V-MCM-41	922	1.79	2.97	2.10
3V-TUD-1	706.6	1.15	5.40	2.02
3V-SBA-15	834.8	1.20	6.04	1.42

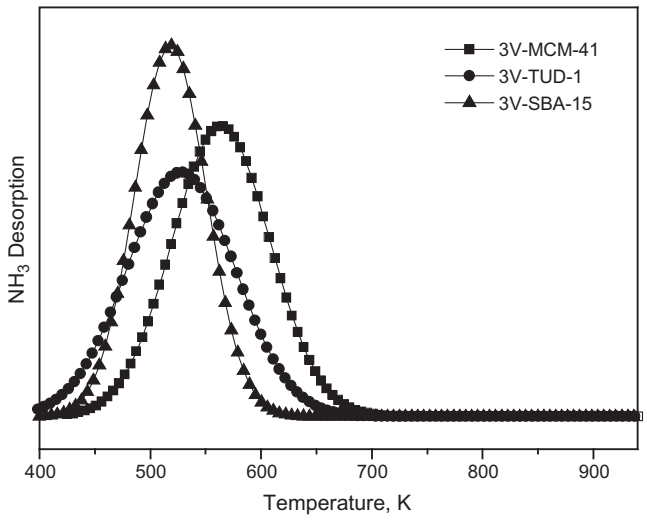

Fig. 3. TPD profiles of 3V-MCM-41, 3V-TUD-1 and 3V-SBA-15.

maximum is located at 519, 526 and 564 K for 3V-SBA-15, 3V-TUD-1 and 3V-MCM-41, respectively. These desorption peaks suggest the existence of weak acid sites with slightly different acid strength [25]. The change in acid strength might be associated to a radius of curvature effect. Feng et al. [20] observed a radius of curvature effect on the catalytic activity during the acid-catalyzed isomerization of 2-methyl-2-pentene on Al-MCM-41. They reported an apparent variation in acid strength of about a factor 5 as the pore size was decreased by a factor 2. In this contribution, surface grafting method was used to prepare highly dispersed isolated VO_4 units on the pore wall surface. Since the Si–O–V bond angle may change as the pore diameter varies, the stability of these Si–O–V units on the pore wall may be changed, resulting in acid sites with different acid strengths. According to the TPD measurements, the acid strength of these V-grafted catalysts decreases as follows: V-MCM-41 > V-TUD-1 > V-SBA-15. However, the desorption peak areas are similar, indicating that a similar number of acid sites was obtain upon 3% V grafting. Furthermore, the TPD profile suggests a more uniform distribution of acid strength for V-SBA-15 than that for V-MCM-41 and V-TUD-1. This can be ascribed to the facts that V-SBA-15 shows larger pore size than that of V-MCM-41 and more uniform pore size distribution than that of V-TUD-1. This may enhance the dispersion of vanadium precursors on the pore wall surface during the post synthesis grafting.

IR spectroscopy of adsorbed pyridine on supported vanadium oxide surface has been widely used since it is able to distinguish different types of surface acid sites [42–45]. Fig. 4 presents the IR spectra of pyridine adsorption on different vanadium grafted catalysts with the same vanadium content (3 wt.%) after desorption at different temperatures. IR bands centered at 1608, 1574, 1489 and 1448 cm^{-1} have been assigned to the 8a and b, 19a and b vibrational modes of pyridine coordinated to Lewis acid sites, respectively [42,45]. Whereas the bands at 1640 (ν8a), 1574 (ν8b), 1489 (ν19a) and 1544 cm^{-1} (ν8b) correspond to pyridinium ions bonded to Brønsted acid sites. The bands at 1489 (ν19a) and 1574 cm^{-1} (ν8b) are associated simultaneously to both Brønsted and Lewis acid sites. In addition to these bands, after desorption at 323K and 373K, the IR spectra also show a peak at 1596 cm^{-1} corresponding to physisorbed pyridine [44,45]. The intensities of all these bands decrease when the desorption temperature increases.

The Lewis and Brønsted acid sites at 1448 and 1544 cm^{-1}, respectively, are generally employed to compare the acid properties, i.e. the acid site density and strength. Following the method developed by Emeis [46], the amount of Lewis and Brønsted acid

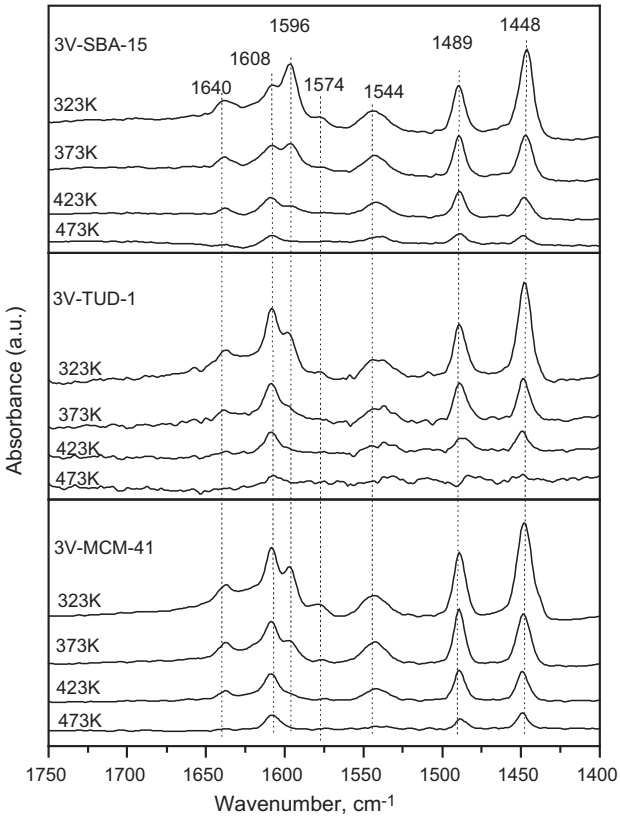

Fig. 4. IR spectra of pyridine adsorption at different temperature for 3V-MCM-41, 3V-TUD-1 and 3V-SBA-15.

sites and the Lewis/Brønsted acidity ratio for different vanadium grafted catalysts are compared. In general, both Lewis and Brønsted acid site densities decrease as the temperature increases. Furthermore, a decrease of the Lewis/Brønsted acidity ratio is also observed for all samples, which is due to the easier desorption of pyridine adsorbed on the Lewis acid sites at elevated temperature as compared to pyridine adsorbed on Brønsted acid sites [47]. The Lewis/Brønsted acidity ratio for each catalyst at the temperature 323 K is shown in Table 1. It is interesting that the Lewis/Brønsted acidity ratio of 3V-SBA-15 is remarkably lower than that of 3V-MCM-41 and 3V-TUD-1 under the same condition, indicating more abundant Brønsted acid sites on 3V-SBA-15 as compared to 3V-MCM-41 and 3V-TUD-1.

3.2. Catalytic reaction

The main isomerization products for all the reactions are *trans*-2-heptene, *cis*-2-heptene, *trans*-3-heptene, *cis*-3-heptene. Skeletal isomerization was not observed over these catalysts because it required stronger acidity (more carbenium ions character is required in the transition state than for double bond shift isomerization) [17,18]. Also, a small amount of cracking and cyclization products were identified.

The 1-heptene conversion and selectivity towards various products over these vanadium grafted catalysts are shown in Fig. 5. As expected, 1-heptene conversion is increased as temperature increases for all catalysts and the activation energy for 3V-MCM-41, 3V-TUD-1 and 3V-SBA-15 are 33.01, 24.52 and 28.03 kJ/mol, respectively. The selectivity towards isomers shows a slight increase with temperature followed by a rapid decrease at the temperature above 573 K, which is due to the relatively more pronounced cyclization at higher temperature [12]. The selectivity of cracking products varies at a low level around 2% which is

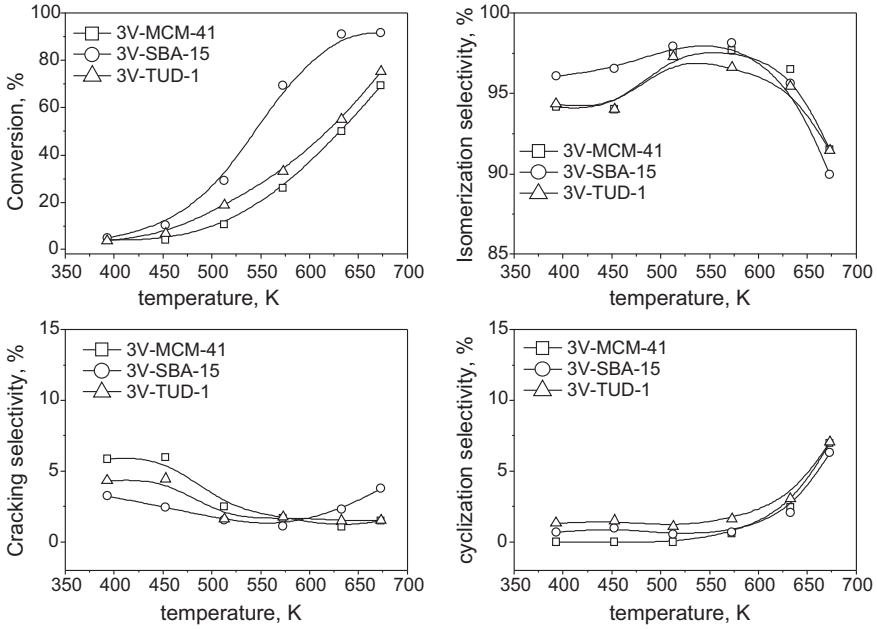

Fig. 5. 1-Heptene isomerization over vanadium grafted catalysts with 3 wt.% vanadium loading.

much less than the reported up to 8% cracking on other catalysts [48]. The sum of cracking and cyclization remains below 10% even at temperatures as high as 673 K, indicating the benefits of these vanadium catalysts in suppressing cyclization and cracking [49]. Among these three studied catalysts, 3V-SBA-15, which has the largest pore size, shows the best conversion of 1-heptene and isomer selectivity at the temperature below 673 K. The conversion increases in the sequence of 3V-MCM-41 < 3V-TUD-1 < 3V-SBA-15. 3V-TUD-1 catalyst with a 3D mesoporous connection, which is proved to benefit for lowering the diffusion resistance in liquid reaction [50], does not show higher conversion than the 2D structural 3V-SBA-15, suggesting the pore diameter (even a slight difference) may play a more crucial role than the pore structure in this particular reaction. Moreover, alkene isomerization is mainly catalyzed by the Brønsted acid sites [18]. As shown in the IR spectra of adsorbed pyridine, the Lewis/Brønsted acidity ratio of 3V-SBA-15 is lower than that of 3V-MCM-41 and 3V-TUD-1. Therefore, it is also reasonable to attribute the high catalytic activity of 3V-SBA-15 to the higher amount of surface Brønsted acid sites.

To further investigate the effect of pore size and pore structure on catalytic performance, the ratios of 2-heptene to 3-heptene (2-HP/3-HP) over these three catalysts are compared in Fig. 6(a). The 2-HP/3-HP ratio decreases with increasing temperature, suggesting high temperature favors the formation of 3-heptene more than 2-heptene, which is in accordance with the thermodynamics study in alkene isomerization [23]. This 2-HP/3-HP ratio varies from 4.3

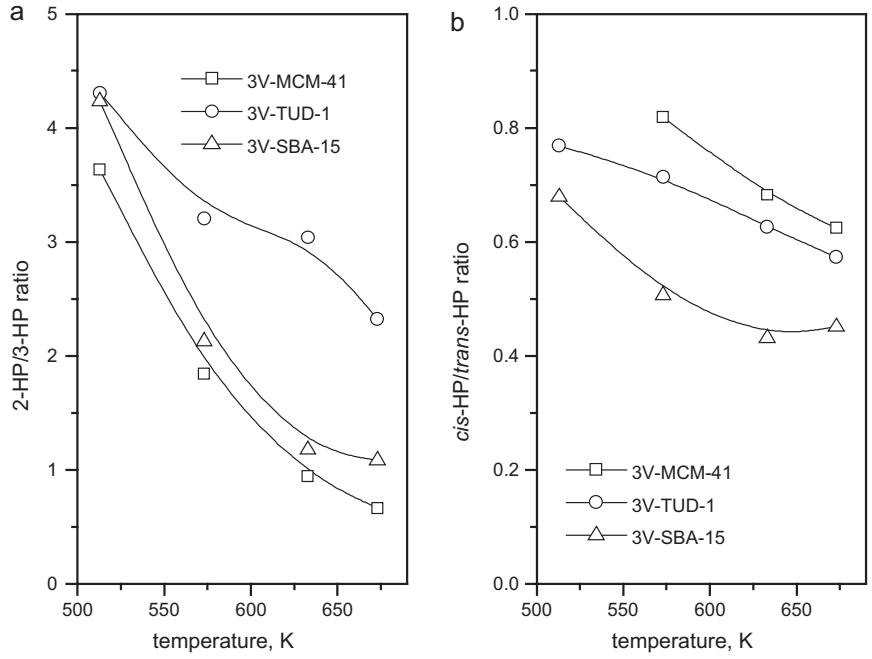

Fig. 6. (a) 2-HP/3-HP and (b) *cis*-HP/*trans*-HP ratios over vanadium grafted catalysts with 3 wt.% vanadium loading.

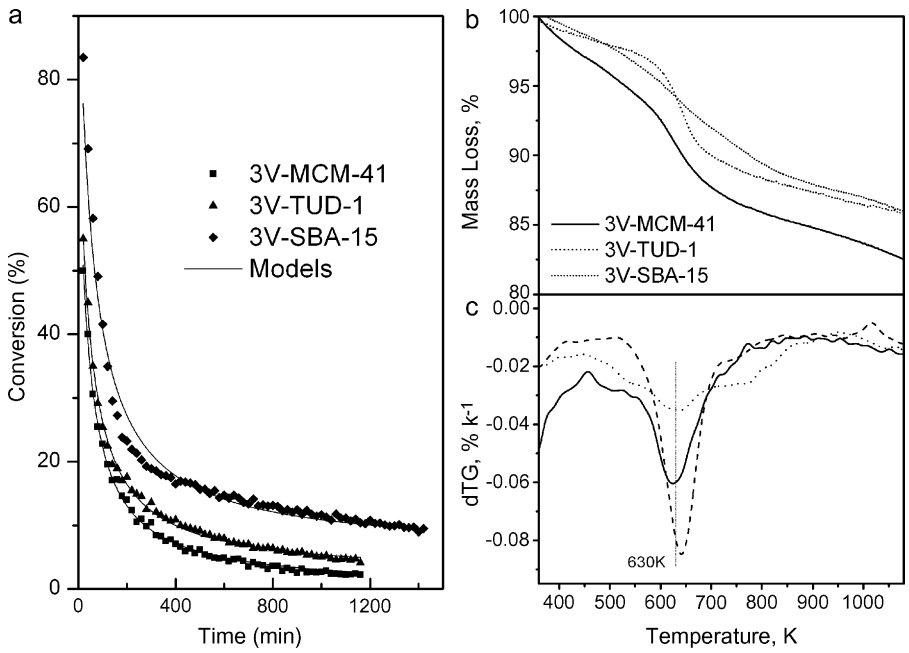

Fig. 7. (a) Catalyst deactivation, (b) thermal analysis and (c) differential thermal analysis of spent catalysts: 3V-MCM-41, 3V-SBA-15 and 3V-TUD-1 after 24 h time-on-stream under 573 K.

to 2.3 for 3V-TUD-1, whereas it changes from 4.3 to 1.1, from 3.6 to 0.7 for 3V-SBA-15 and 3V-MCM-41, respectively. Most of the values are greater than 1, which maybe explained as the 3-heptene precursor $CH_2H_5–C^+H–C_3H_7$ carbenium ion is formed by the hydride transfer from the precursor of 2-heptene $CH_3–C^+H–C_4H_9$ carbenium ion [51]. The 2-HP/3-HP ratio over 3V-TUD-1 is always higher than that on 3V-SBA-15 and 3V-MCM-41. It is suggested that the formed 2-heptene is able to diffuse out the catalyst quickly in the 3D structure of 3V-TUD-1, while 2D structure of 3V-SBA-15 and 3V-MCM-41 may linger the 2-heptene in the channels relatively longer and rearrange 2-heptene into 3-heptene due to the hydride transfer. The diffusion limitation may also explain why the 2-HP/3-HP ratio over SBA-15 is slightly higher than MCM-41 which possesses a smaller pore size.

The ratio of *cis*-heptene to *trans*-heptene (*cis*-HP/*trans*-HP) varies with temperature over these catalysts. As shown in Fig. 6(b), all the *cis*-HP/*trans*-HP ratio values are less than 1, implying the *trans*-type isomer is relatively easier to be formed. The *cis*-HP/*trans*-HP ratio decreases along the reaction temperature, indicating the *cis*-type isomer may transform into a *trans*-type isomer at elevated temperature. Rao et al. [17] reported larger pore diameter showed larger *cis*-HP/*trans*-HP ratio in zeolites due to the reason that large pores have less resistance for *cis*-alkene to diffuse out. Nevertheless, it may not be applicable in mesoporous materials as the pore sizes are much larger than those of zeolites. The *cis*-HP/*trans*-HP ratios in mesoporous catalysts show an opposite trend, lowest *cis*-HP/*trans*-HP ratio is observed over 3V-SBA-15, whereas 3V-MCM-41 shows the highest value which has the smallest pore diameter. As the carbenium ions rearrangement occurs during the reaction [51], catalyst with larger pore size may provide more space for *cis*-heptene to transform into the more steric stable *trans*-heptene, resulting in the decrease of the *cis*-HP/*trans*-HP ratio with the pore size. Kissin [51] has suggested the empirical calculation that the ratio of *cis*/*trans* isomers is around 0.47 for any alkene with an internal C=C bond, which is close to the thermodynamic equilibrium content. In this study, the *cis*-HP/*trans*-HP ratio over 3V-SBA-15 is between 0.43 and 0.51 in the temperature range of 573 to 673 K, which is close to this empirical value. This further confirms that the larger pore size let the *cis*-HP/*trans*-HP ratio closer to the intrinsic thermodynamic equilibrium ratio, and smaller pore size would limit the transform from *cis*-HP to *trans*-HP.

Different carrier gases were investigated in the isomerization of alkene. Hydrogen was observed to slow down the catalyst deactivation during the isomerization of 1-hexene [12]. However, hydrogen may cause the formation of hydrogenation products which still lowered the octane number of the products [12,25]. In this study, helium was employed as the carrier gas and the deactivation of the catalysts was studied.

Fig. 7(a) clearly shows that the catalytic activity declines as a function of time-on-stream, which is in good agreement with the literature [17,18]. During the reaction, alkene can easily form coke precursors, which may lead to catalyst deactivation. To quantify the deactivation rate, the experimental data were fitted using a simple deactivation model. Fig. 7(a) seems to indicate that the catalytic activity reaches a pseudo-steady state activity, usually named as residual activity. As indicated by Monzon et al. [52], when the catalysts exhibit residual activity, more general models to predict the presence of this residual activity should be used. Eq. (1) is frequently used to describe deactivation data with residual activity [51]:

$$-\frac{da}{dt} = \psi_d (a - a_{ss})^d \quad (1)$$

Table 2
Deactivation parameters of vanadium grafted catalysts.

Sample	Initial conversion (%)	Deactivation constant, ψ_d (min^{-1})	Residual activity, a_{ss}	Statistical parameter (R^2)
3V-MCM-41	75.0	0.024	0 (X_{ss} = 0%)	0.9966
3V-TUD-1	78.2	0.022	0.025 (X_{ss} = 2.5%)	0.9964
3V-SBA-15	100	0.018	0.055 (X_{ss} = 5.5%)	0.9759

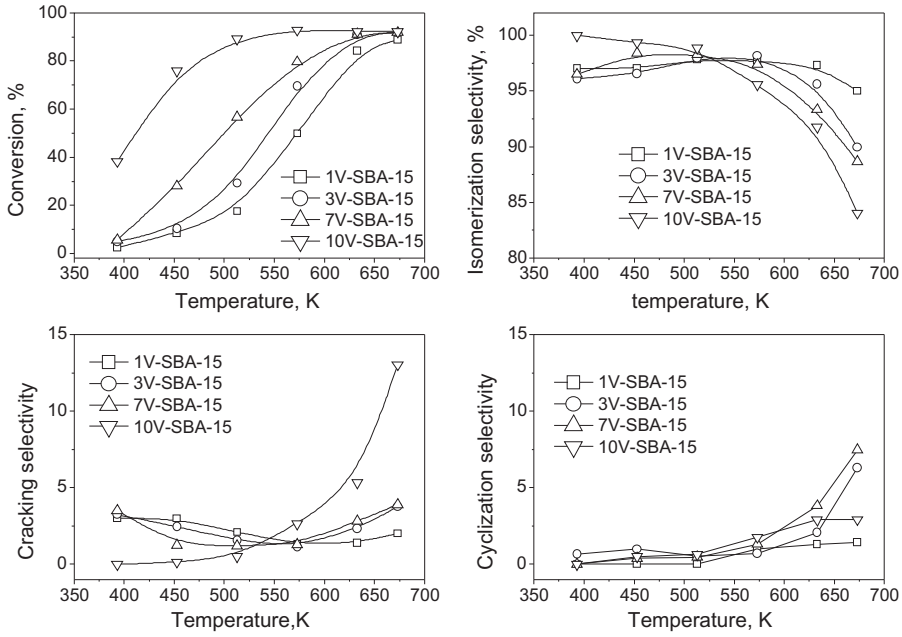

Fig. 8. 1-Heptene isomerization reaction over V-SBA-15 catalysts with different vanadium loadings.

where a is the catalytic activity:

$$a_{(t)} = \frac{r_{(t)}}{r_0} \tag{2}$$

ψ_d is the deactication function, d is the deactivation order and a_{ss} is the residual activity.

As shown in Fig. 7(a), the deactivation curves are satisfactorily fitted using a 2nd order deactivation model. Table 2 summarizes the kinetic deactivation parameters. Although all samples exhibit a significant deactivation, the 3%V-SBA-15 catalyst shows a slight better deactivation behavior, both in terms of deactivation constant and residual activity.

Fig. 7(b) shows the thermogravimetric results of spent 3V-MCM-41, 3V-SBA-15 and 3V-TUD-1 catalysts after the stability tests. The corresponding differential thermal analysis is shown in Fig. 7(c). The small weight loss before 600 K is due to the desorption of reactants and products adsorbed in the pores. The surface area decreases in the sequence of 3V-MCM-41 > 3V-SBA-15 > 3V-TUD-1, the amount of reactant and products adsorbed on the catalysts also follows the same trend. The significant weight loss around 630 K is mainly caused by the oxidation of carbonaceous species [53]. The amount of coke on these three catalysts decreases in the order 3V-TUD-1 > 3V-MCM-41 > 3V-SBA-15. This may be again due to the larger pore size of V-SBA-15 provides better diffusion for the reactants and products and thus formed less coke.

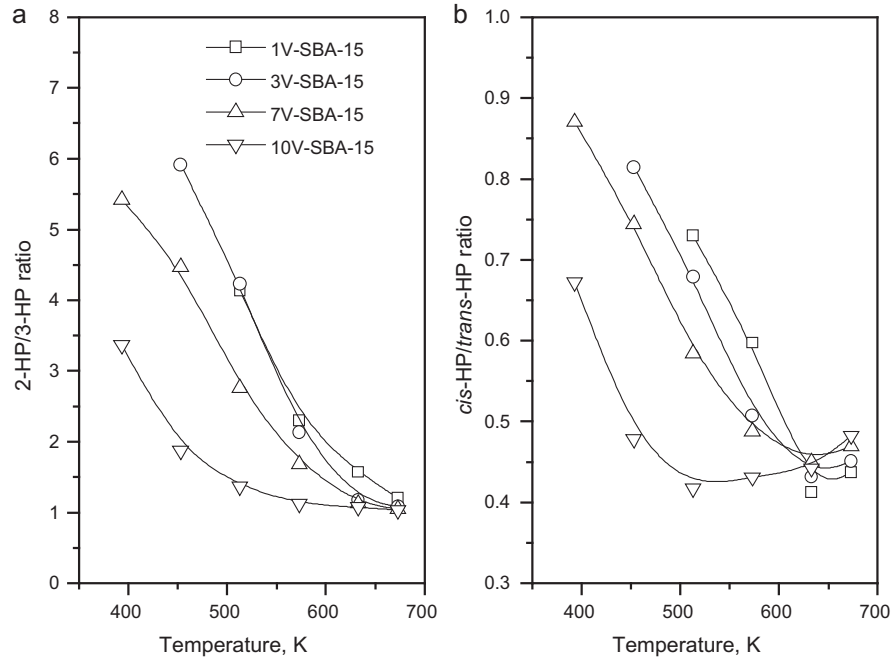

Fig. 9. (a) 2-HP/3-HP and (b) *cis*-HP/*trans*-HP ratios over V-SBA-15 catalysts with different vanadium loadings.

As 3V-SBA-15 shows the best catalytic performance and lowest deactivation rate among these catalysts, vanadium content is changed over SBA-15 support to investigate the vanadium loading effect. Results of 1-heptene isomerization over V-SBA-15 catalysts with different vanadium contents varying from 1 to 10 wt.% are shown in Fig. 8. The conversion increases along the temperature, a higher vanadium content leads to a higher conversion as expected. For instance, at 513 K, the conversions are 17.5%, 29.2%, 56.7% and 90.7% for 1V-SBA-15, 3V-SBA-15, 7V-SBA-15 and 10V-SBA-15, respectively. The isomer selectivity remains above 95% in the temperatures range from 393 to 573 K, followed by an abrupt decrease at temperatures above 573 K, which is also due to the pronounced cyclization at high temperatures. The isomer selectivity on 1V-SBA-15 remains above 95% at all the temperatures tested in this study. The isomer selectivity decreases more rapidly for the V-SBA-15 catalysts with a higher vanadium content when the reaction temperature is above 573 K due to the pronounced cracking and cyclization side reactions.

The dependence of 2-HP/3-HP ratio on temperature over V-SBA-15 is shown in Fig. 9(a). The 2-HP/3-HP ratio over different V-SBA-15 catalysts decreases with the temperature. The 2-HP/3-HP ratio decreases as the vanadium content is increased. For example, the 2-HP/3-HP ratios are 2.3, 2.1, 1.7, 1.1 for 1V-SBA-15, 3V-SBA-15, 7V-SBA-15 and 10V-SBA-15, respectively. The correlations between 2-HP/3-HP ratio and the vanadium content suggests that not only the pore structure plays a role, but also the vanadium content has an impact upon the product distributions. High content of vanadium forms more active sites, which may promote the transformation of 2-heptene into 3-heptene. At high temperature of 673 K, the 2-HP/3-HP ratio reaches its equilibrium value around 1.1 for all these V-SBA-15 catalysts. The temperature effect on the *cis*-HP/*trans*-HP ratio over different V-SBA-15 catalysts is shown in Fig. 9(b). All the *cis*-HP/*trans*-HP ratios are less than 1. The *cis*-HP/*trans*-HP ratio shows a remarkable decrease at low temperatures followed by a plateau at high temperatures. Within the studied temperature range between 393 and 633 K, the *cis*-HP/*trans*-HP ratio decreases with the increase of the vanadium content. For instance, the *cis*-HP/*trans*-HP ratios are 0.60, 0.51, 0.49, 0.43 for 1V-SBA-15, 3V-SBA-15, 7V-SBA-15 and 10V-SBA-15, respectively, which may be due to more active sites increase the possibility of *cis*-heptene rearranging into more steric stable *trans*-heptene.

4. Conclusions

Highly dispersed vanadium active sites over different mesoporous supports were obtained via the ALD grafting method. Characterization techniques were employed to study the pore size and structure of the mesoporous supports, the coordination state of vanadium and the acid properties of the resulting catalysts. The results show a significant effect of both pore structure and size on the catalytic performance during 1-heptene isomerization. Larger pore size exhibits higher conversion and lower *cis*-HP/*trans*-HP ratio. V-TUD-1, a mesoporous material with 3D pore structure, shows higher 2-HP/3-HP ratio than 2D structural V-MCM-41 and V-SBA-15 samples. Seen that the best catalytic performance can be achieved using SBA-15 as support, V-SBA-15 samples with varying V loading were investigated. Higher V content results in higher conversion, lower 2-HP/3-HP ratio and lower *cis*-HP/*trans*-HP ratio, although it may cause a slight decrease in the isomer selectivity. Catalyst stability tests indicate that V-SBA-15 exhibits the lowest deactivation rate and less coke formation, which can be probably ascribed to the largest pore diameter.

Acknowledgement

Funding from the Singapore Agency for Science, Technology and Research (A*STAR), SERC Grant No: 102 101 0020 in support of this project is gratefully acknowledged.

References

[1] H. Li, M. Li, Y. Chu, H. Nie, Micropor. Mesopor. Mater. 117 (2009) 635–639.
[2] M. Mehl, G. Vanhove, W.J. Pitz, E. Ranzi, Combust. Flame 155 (2008) 756–772.
[3] K.R. Sawyer, E.A. Glascoe, J.F. Cahoon, J.P. Schlegel, C.B. Harris, Organometallics 27 (2008) 4370–4379.
[4] B. de Menorval, P. Ayrault, N.S. Gnep, M. Guisnet, J. Catal. 230 (2005) 38–51.
[5] B. de Menorval, P. Ayrault, N.S. Gnep, M. Guisnet, Appl. Catal. A: Gen. 304 (2006) 1–13.
[6] G. Erdogan, D.B. Grotjahn, J. Am. Chem. Soc. 131 (2009) 10354–10355.
[7] J. Guo, X.W. Cheng, W.Z. Zhou, Y.C. Long, Micropor. Mesopor. Mater. 79 (2005) 319–328.
[8] M. Tiitta, E. Harlin, J. Makkonen, A. Root, F. Sandelin, H. Osterholm, Recent Advances in the Science and Technology of Zeolites and Related Materials, Pts a – C, 2004, pp. 2323–2330.
[9] D.D. Li, M.F. Li, Y. Chu, H. Nie, Y.H. Shi, Catal. Today 81 (2003) 65–73.
[10] D.B. Grotjahn, C.R. Larsen, J.L. Gustafson, R. Nair, A. Sharma, J. Am. Chem. Soc. 129 (2007) 9592–9593.
[11] S.A. Goddard, S.G. Kukes, Energ. Fuels 8 (1994) 147–150.
[12] B. Modhera, M. Chakraborty, P.A. Parikh, H.C. Bajaj, Catal. Lett. 132 (2009) 168–173.
[13] G. Shi, J. Shen, Energ. Fuels 23 (2008) 320–326.
[14] D. Li, M. Li, Y. Chu, H. Nie, Y. Shi, Catal. Today 81 (2003) 65–73.
[15] C. Yin, R. Zhao, C. Liu, Fuel 84 (2005) 701–706.
[16] M. Toba, Y. Miki, T. Matsui, M. Harada, Y. Yoshimura, Appl. Catal. B: Environ. 70 (2007) 542–547.
[17] Y. Rao, J. Kang, D. Antonelli, J. Am. Chem. Soc. 130 (2007) 394–395.
[18] Y. Rao, J. Kang, M. Trudeau, D.M. Antonelli, J. Catal. 266 (2009) 1–8.
[19] A. Corma, V. Fornes, M.T. Navarro, J. Perezpariente, J. Catal. 148 (1994) 569–574.
[20] X. Feng, J.S. Lee, J.W. Lee, D. Lee, D. Wei, G.L. Haller, Chem. Eng. J. 64 (1996) 255.
[21] Y.H. Yang, G.A. Du, S.Y. Lim, G.L. Haller, J. Catal. 234 (2005) 318–327.
[22] Q. Tang, C. Wang, S. Hu, H. Sun, Y. Chen, G. Haller, Y. Yang, Catal. Lett. 117 (2007) 25–33.
[23] J. Abbot, A. Corma, B.W. Wojciechowski, J. Catal. 92 (1985) 398–408.
[24] M.R. Prasad, G. Madhavi, A.R. Rao, S.J. Kulkarni, K.V. Raghavan, J. Porous Mater. 13 (2006) 81–94.
[25] S. Hu, D. Liu, L. Li, A. Borgna, Y. Yang, Catal. Lett. 129 (2009) 478–485.
[26] P. Wehrer, S. Libs, L. Hilaire, Appl. Catal. A: Gen. 238 (2003) 69–84.
[27] G. Du, S. Lim, M. Pinault, C. Wang, F. Fang, L. Pfefferle, G.L. Haller, J. Catal. 253 (2008) 74–90.
[28] Y.C. Lou, Q.H. Tang, H.R. Wang, B.T. Chia, Y. Wang, Y.H. Yang, Appl. Catal. A: Gen. 350 (2008) 118–125.
[29] M.S. Hamdy, A. Ramanathan, T. Maschmeyer, U. Hanefeld, J.C. Jansen, Chem. Eur. J. 12 (2006) 1782–1789.
[30] A. Corma, Chem. Rev. 97 (1997) 2373–2420.
[31] A. Vinu, D.P. Sawant, K. Ariga, K.Z. Hossain, S.B. Halligudi, M. Hartmann, M. Nomura, Chem. Mater. 17 (2005) 5339–5345.
[32] Z. Shan, J.C. Jansen, W. Zhou, T. Maschmeyer, Appl. Catal. A: Gen. 254 (2003) 339–343.
[33] J.C. Jansen, Z. Shan, L. Marchese, W. Zhou, N. von der Puil, T. Maschmeyer, Chem. Commun. (2001) 713–714.
[34] R. Schmidt, E.W. Hansen, M. Stoecker, D. Akporiaye, O.H. Ellestad, J. Am. Chem. Soc. 117 (1995) 4049–4056.
[35] S. Shylesh, A.R. Singh, J. Catal. 244 (2006) 52–64.
[36] B. Solsona, T. Blasco, J.M.L. Nieto, M.L. Pena, F. Rey, A. Vidal-Moya, J. Catal. 203 (2001) 443–452.
[37] N. Das, H. Eckert, H.C. Hu, I.E. Wachs, J.F. Walzer, F.J. Feher, J. Phys. Chem. 97 (1993) 8240–8243.
[38] A. Davidson, M. Che, J. Phys. Chem. 96 (1992) 9909–9915.
[39] G.T. Went, S.T. Oyama, A.T. Bell, J. Phys. Chem. 94 (1990) 4240–4246.
[40] H. Tian, E.I. Ross, I.E. Wachs, J. Phys. Chem. B 110 (2006) 9593–9600.
[41] L. Rodríguez-González, F. Hermes, M. Bertmer, E. Rodríguez-Castellón, A. Jiménez-López, U. Simon, Appl. Catal. A: Gen. 328 (2007) 174–182.
[42] Q. Sun, Y. Fu, J. Liu, A. Auroux, J. Shen, Appl. Catal. A: Gen. 334 (2008) 26–34.
[43] T. Blasco, A. Galli, J.M. López Nieto, F. Trifiró, J. Catal. 169 (1997) 203–211.
[44] F. Hatayama, T. Ohno, T. Maruoka, T. Ono, H. Miyata, J. Chem. Soc. Faraday Trans. 87 (1991) 2629–2633.
[45] J. Keränen, A. Auroux, S. Ek, L. Niinistö, Appl. Catal. A: Gen. 228 (2002) 213–225.
[46] C.A. Emeis, J. Catal. 141 (1993) 347–354.
[47] S. Lim, G.L. Haller, J. Phys. Chem. B 106 (2002) 8437–8448.
[48] R. Roldán, F.J. Romero, C. Jiménez-Sanchidrián, J.M. Marinas, J.P. Gómez, Appl. Catal. A: Gen. 288 (2005) 104–115.
[49] J.S. Buchanan, J.G. Santiesteban, W.O. Haag, J. Catal. 158 (1996) 279–287.
[50] M.C.C. Anand Ramanathan, C. Villalobos, S. Kwakernaak, U. Telalovic, Hanefeld, Chem. Eur. J. 14 (2008) 961–972.
[51] Y.V. Kissin, Catal. Rev. Sci. Eng. 43 (2001) 85–146.
[52] A. Monzon, E. Romeo, A. Borgna, Chem. Eng. J. 94 (2003) 19–28.
[53] X. Guo, Y. Zheng, B. Zhang, J. Chen, Biomass Bioenerg. 33 (2009) 1469–1473.